

Revisiting the Hybrid Quantum Monte Carlo Method for Hubbard and Electron-Phonon Models.

Stefan Beyl, Florian Goth, and Fakher F. Assaad

*Institut für Theoretische Physik und Astrophysik,
Universität Würzburg, Am Hubland, D-97074 Würzburg, Germany*

(Dated: May 15, 2022)

A unique feature of the Hybrid Quantum Monte Carlo (HQMC) method is the potential to simulate negative sign free lattice fermion models with sub-cubic scaling in system size. Here we will revisit the algorithm for various models. We will show that for the Hubbard model the HQMC suffers from ergodicity issues and unbounded forces in the effective action. Solutions to these issues can be found in terms of a complexification of the auxiliary fields, but nevertheless, the HQMC approach does not outperform single spin flip determinantal methods with cubic scaling. On the other hand we will argue that there is a set of models for which the HQMC is very efficient. This class is characterized by effective actions free of singularities. Using the Majorana representation, we show that models such as the Su-Schrieffer-Heeger Hamiltonian at half-filling and on a bipartite lattice belongs to this class. For this specific model sub-cubic scaling is achieved.

PACS numbers: 02.70.Ss, 63.20.kd, 71.10.Fd

CONTENTS

I. Introduction	1
II. HQMC for the Hubbard model	2
A. Basic formalism	2
B. The Hybrid Monte Carlo updating scheme	3
C. Detailed balance - the right choice of the integrator	4
D. Evaluation of the forces and measurement of observables	4
E. Solution of linear systems with the conjugate gradient method	5
F. Ergodicity issues	7
III. Complex reformulation and Comparison	7
A. Complexification	7
B. Results of the complex method	9
C. Comparison between cHQMC and BSS for the Hubbard model	9
IV. HQMC and the SSH model	10
A. HQMC formulation for the SSH model	10
B. Proof of Concept	11
V. Conclusion	12
Acknowledgments	13
References	13

extremely interesting phases of matter and quantum phase transitions^{5–11}. Since in a lot of these models the fermions are gapless, they cannot be integrated out, and are at the very origin of novel quantum critical phenomena^{12–18}. From the technical point of view, this leads to the necessity of developing efficient algorithms for lattice fermions so as to unravel facets of fermion critical phenomena in two and higher spacial dimensions.

The condensed matter community has focused on the Blankenbecler Scalapino Sugar (BSS) auxiliary field determinantal QMC technique^{19–21}. This approach invariably scales as the cubed of the volume since the fermionic determinant is explicitly calculated. Furthermore, since the determinant is non-local, cluster algorithms have remained elusive and single spin-flip updates are still the standard. Using machine learning techniques to propose global moves is an ongoing active research subject^{22–24}. On the other hand, in particle physics, especially in the lattice gauge theory community, the Hybrid Quantum Monte Carlo method (HQMC) was used and extended^{25–27}. A glimpse at the simulated system sizes fosters the hope to access larger lattice sizes, at least for a selected subset of models, by using HQMC. From a conceptual point of view, the HQMC method offers two main advantages in comparison to established methods in the condensed matter:

- A global updating scheme, based on Hamilton's equations of motion²⁸, that guarantees a good acceptance rate.
- Replacing determinants by gaussian integrals is the first key step to allow for sub-cubic scaling.

I. INTRODUCTION

There has recently been tremendous progress in classifying fermionic model Hamiltonians that one can solve with quantum Monte Carlo (QMC) methods without encountering the infamous negative sign problem^{1–4}. Remarkably, this class of models contains a number of

Note that global update schemes such as Langevin dynamics or Hybrid Monte Carlo²⁸ can be implemented in schemes that explicitly retain the fermion determinant.

The structure and main results of this article are as follows. In Sec. II we will revisit the ideas of Ref. 25

as applied to the Hubbard model. A number of subsections will give us the opportunity to introduce notation and summarize important ideas of the HQMC. In the final subsection, IIF, we show that the algorithm is not ergodic, even at half-filling when the weight is always positive. The fermion determinant in each spin sector has a strongly fluctuating sign at low temperatures. Particle-hole symmetry locks the relative signs of the determinants to unity and the weight is positive. Nevertheless, at low temperatures the weight has many zero modes and different regions of configuration space are separated by divergences in the effective potential through which the molecular dynamics cannot tunnel. In Sec. III we proceed to describe a complexification of the algorithm that circumvents these ergodicity issues. In contrast to Ref. 29 our approach is based on a complex Hubbard Stratonovich (HS) transformation. In Subsection III C we show that an ergodic algorithm can be achieved and that it can reproduce standard BSS results as obtained with the ALF-package³⁰. However, for the Hubbard model, the HQMC does not provide an improved scaling and is less efficient in terms of fluctuations. Here we note that the BSS relies on a discrete Hubbard-Stratonovich transformation, thereby circumventing the above ergodicity issues.

To proceed we will ask the question if there is a class of models in the solid state for which the HQMC can be the method of choice. To do so, we will follow the idea that the Hubbard model is hard, since the effective action shows divergences and thereby generates forces that are unbounded. With the help of recent progress in our understanding of the negative sign problem²⁻⁴, it can be shown that for a class of models the fermion determinant in a single spin sector is positive semi-definite. This turns out to be the case for the so called n -flavored Su-Schrieffer-Heeger (SSH) model³¹ at half-filling and on any bipartite lattice. We have implemented the HQMC for this model and have benchmarked our results against the so-called continuous time interaction expansion (CT-INT) algorithm³²⁻³⁴ where the phonons are integrated out in favor of a retarded interaction. It appears that this model can be efficiently simulated with the HQMC. For the comparison with other approaches, two points are in order. i) There is by construction no discrete-field formulation of this model, and local moves lead to large autocorrelation times³⁵ and ii) although very appealing, the CT-INT approach suffers from a negative sign problem at finite phonon frequency and in dimensions larger than unity. We will hence conclude and give numerical evidence in Sec. IV that the HQMC could be the method of choice for this specific model Hamiltonian. It is also interesting to note that the SSH model, in some limiting cases, maps onto a Z_2 lattice gauge theory as pointed out in Ref. 10. Finally Sec. V draws some conclusions.

II. HQMC FOR THE HUBBARD MODEL

We start with a pedagogical introduction to the HQMC method in condensed matter systems by revisiting Scalettar's²⁵ initial formulation. This will provide us with the necessary background to discuss failures and means to resolve them. At the end of the section, we will discuss ergodicity issues.

A. Basic formalism

The Hubbard Hamiltonian \hat{H} is given as the sum of a kinetic part \hat{H}_K and an interacting part \hat{H}_U ,

$$\hat{H} = \hat{H}_K + \hat{H}_U. \quad (1)$$

While the kinetic energy is given by a tight binding Hamiltonian

$$\hat{H}_K = -t \sum_{\langle i,j \rangle, \sigma} \left(\hat{c}_{i,\sigma}^\dagger \hat{c}_{j,\sigma} + \hat{c}_{j,\sigma}^\dagger \hat{c}_{i,\sigma} \right) \quad (2)$$

and favors extended states, the potential energy is represented by an on-site Hubbard interaction

$$\hat{H}_U = U \sum_i \left(\hat{n}_{i,\uparrow} - \frac{1}{2} \right) \left(\hat{n}_{i,\downarrow} - \frac{1}{2} \right), \quad (3)$$

and favors localized states. $\hat{c}_{i,\sigma}^\dagger$ ($\hat{c}_{i,\sigma}$) denote fermionic operators that create (annihilate) an electron in a Wannier state centered around site i with z -component of spin σ and $\langle i,j \rangle$ denotes nearest neighbors of a hyper cubic lattice. The Hubbard interaction strength is given by U , t denotes the hopping matrix element and $\hat{n}_{i,\sigma} = \hat{c}_{i,\sigma}^\dagger \hat{c}_{i,\sigma}$. To describe thermodynamical properties, the partition function Z is the quantity of interest. To compute it we discretize the imaginary time τ and introduce a Trotter-decomposition

$$\begin{aligned} Z &= \text{tr} e^{-\beta \hat{H}} \\ &= \text{tr} \left(e^{-\Delta_\tau \hat{H}} \right)^{N_\tau} \\ &\simeq \text{tr} \left(e^{-\Delta_\tau \hat{H}_K} e^{-\Delta_\tau \hat{H}_U} \right)^{N_\tau}. \end{aligned} \quad (4)$$

Here $N_\tau \Delta_\tau = \beta$. The discretization into Δ_τ slices is common to the HQMC and the BSS-QMC. For the sake of comparison, it is important to note that both methods share the same Δ_τ discretization error. To be able to integrate out the fermions, we have to decouple the many body interaction term into a sum of single body propagators. This is achieved with a Hubbard-Stratonovich (HS) decomposition that introduces an auxiliary field $x_{i,l}$ at each site i and every time slice l ,

$$\exp \left[-\Delta_\tau U \left(\hat{n}_{i,\uparrow} - \frac{1}{2} \right) \left(\hat{n}_{i,\downarrow} - \frac{1}{2} \right) \right] = (\Delta_\tau / \pi)^{1/2} e^{-\Delta_\tau U/4} \int_{-\infty}^{\infty} dx_{i,l} \exp \left\{ -\Delta_\tau \left[x_{i,l}^2 + \sqrt{2U} x_{i,l} (\hat{n}_{i,\uparrow} - \hat{n}_{i,\downarrow}) \right] \right\}. \quad (5)$$

In contrast to the discrete auxiliary field of the BSS-algorithm^{30,36} this field is continuous. At this point, we can integrate out the fermion degrees of freedom to obtain:

$$Z = \int [\delta x] e^{-S_B(x)} \det M_\uparrow(x) \det M_\downarrow(x), \quad (6)$$

where we have introduced the shorthand notation for the action of the auxiliary fields

$$S_B(x) := \Delta_\tau \sum_{i,l} x_{i,l}^2. \quad (7)$$

The matrices $M_\sigma(x)$, appearing in the determinants, have a block structure:

$$M_\sigma = \begin{pmatrix} I & 0 & 0 & \cdots & 0 & B_{N_\tau, \sigma} \\ -B_{1, \sigma} & I & 0 & \cdots & 0 & 0 \\ 0 & -B_{2, \sigma} & I & \cdots & 0 & 0 \\ \vdots & \vdots & \vdots & \ddots & \vdots & \vdots \\ 0 & 0 & 0 & \cdots & I & 0 \\ 0 & 0 & 0 & \cdots & -B_{N_\tau-1, \sigma} & I \end{pmatrix}. \quad (8)$$

The dimension, $V_S \times V_S$, of the block matrices is determined by the number of sites V_S . In the above,

$$B_{l, \sigma}(x) = e^{-\Delta_\tau K} e^{-\sigma \Delta_\tau V_{l, \sigma}(x)}. \quad (9)$$

K represents the tight binding hopping matrix with elements

$$K_{i,j} = \begin{cases} -t & \langle i, j \rangle \text{ nearest neighbors} \\ 0 & \text{otherwise} \end{cases}, \quad (10)$$

and the diagonal matrix V contains the fields

$$(V_l)_{i,j}(x) = \delta_{i,j} \sqrt{2U} x_{i,l}. \quad (11)$$

Eq. (6) provides a suitable representation for discussing the absence of the fermionic sign problem. For a half-filled bipartite lattice, where hopping occurs only between the two sublattices, it can be shown that both determinants have always the same sign since under a particle-hole transformation:

$$\det M_\downarrow(x) = e^{-\Delta_\tau \sqrt{2U} \sum_{i,l} x_{i,l}} \det M_\uparrow(x). \quad (12)$$

Thus, at half-filling the fermionic sign problem is absent, since all configurations of the auxiliary field have a positive statistical weight³⁷. One of the key steps to avoid cubic scaling is to get rid of the determinant and to sample it stochastically. To this aim, one introduces so-called pseudo fermion fields ϕ_σ to obtain

$$Z = \int [\delta x \delta \phi_\sigma] e^{-S_B(x) - \sum_\sigma \phi_\sigma^T (M_\sigma^T(x) M_\sigma(x))^{-1} \phi_\sigma}. \quad (13)$$

Clearly the above implicitly assumes the absence of negative sign problem, $\det M_\uparrow(x) \det M_\downarrow(x) > 0$.

B. The Hybrid Monte Carlo updating scheme

This subsection summarizes Hybrid Monte Carlo sampling. Details on the implementation will be given at the end of this subsection. In order to define a Hamiltonian system, we add a canonical conjugate variable, $p_{i,l}$, to the HS field such that Eq. (13) reads:

$$Z = \int [\delta x \delta p \delta \phi_\sigma] P(x, p, \phi_\sigma) \quad (14)$$

with the distribution function

$$P(x, p, \phi_\sigma) = e^{-\mathcal{H}(x, p, \phi_\sigma)} \quad (15)$$

and Hamiltonian

$$\begin{aligned} \mathcal{H}(x, p, \phi_\sigma) := & S_B(x) + \sum_{i,l} p_{i,l}^2 + \\ & + \sum_\sigma \phi_\sigma^T (M_\sigma^T(x) M_\sigma(x))^{-1} \phi_\sigma. \end{aligned} \quad (16)$$

We now want to draw samples from the distribution $P(x, p, \phi_\sigma)$ on the state space spanned by the set of continuous variables $\{x, p, \phi_\sigma\}$. The components of the momentum $p_{i,l}$ are distributed according to a gaussian distribution and can be sampled directly. The auxiliary fields ϕ can be sampled in the following way. Given the auxiliary variables

$$R_\sigma := (M_\sigma^T(x))^{-1} \phi_\sigma, \quad (17)$$

drawn from a gaussian distribution, we can obtain ϕ from

$$\phi_\sigma = M_\sigma^T(x) R_\sigma. \quad (18)$$

To sample the field x we use Hamilton's equations of motion based on the Hamilton function of Eq. (16) at fixed values of the pseudo fermion fields:

$$\dot{p}_{i,l} = -\frac{\partial \mathcal{H}}{\partial x_{i,l}} \quad (19)$$

$$\dot{x}_{i,l} = \frac{\partial \mathcal{H}}{\partial p_{i,l}}. \quad (20)$$

Integration over a given time interval yields a new point in phase space, x' and p' , that we will accept according to the Metropolis-Hastings rule:

$$\begin{aligned} r_{\text{MH}} = & \min \left(1, \frac{T_0(x', p' \rightarrow x, p)}{T_0(x, p \rightarrow x', p')} \frac{P(x', p', \phi)}{P(x, p, \phi)} \right) \\ = & \min \left(1, e^{\mathcal{H}(x, p, \phi) - \mathcal{H}(x', p', \phi)} \right), \end{aligned} \quad (21)$$

where T_0 corresponds to the proposal probability density. For the last identity we have used the fact that Hamiltonian dynamics is time reversal symmetric and that the phase space volume is conserved. Under these assumptions, which will have to be satisfied by the numerical integrator (see below), $\frac{T_0(x', p' \rightarrow x, p)}{T_0(x, p \rightarrow x', p')} = 1$. Throwing a random number against r_{MH} we can then decide whether we accept the update. Clearly, if the Hamiltonian propagation is carried out exactly, the acceptance is unity. To conclude this overview we summarize the updating procedure

- draw gaussian samples for $p_{i,l}$ and $R_{\sigma,i,l}$.
- evolve x and p according to Hamilton's equations of motions.
- accept the new values of x and p according to the Metropolis-Hastings ratio.

C. Detailed balance - the right choice of the integrator

As alluded above, to integrate the equations of motion we have to proceed with care and remember that Hamilton's equations of motion have two important properties: first, by Liouville's theorem the phase space volume is conserved, and secondly, they are time reversal symmetric. Under the condition that we choose an integrator for Hamilton's equations of motions for the updates of x and p that retains these properties it follows that our Monte Carlo updates fulfill the detailed balance condition³⁸. Integrators that have these favorable traits are called symplectic, or geometric integrators³⁹ and the most well-known example of them is the Leapfrog method. The Leapfrog method satisfies time reversibility and is well established in numerics. It solves the equation of motion iteratively over an artificial time. The artificial Leapfrog time has to be discretized into time steps Δt . Initially we propagate the momentum field by a half time step $\Delta t/2$. Afterwards we propagate alternatively the spatial field

$$\begin{aligned} x_{i,l}(t + \Delta t) - x_{i,l}(t) &= \int_t^{t+\Delta t} dt' 2p_{i,l}(t') \\ &= 2p_{i,l}\left(t + \frac{1}{2}\Delta t\right) \Delta t + \mathcal{O}(\Delta t^3) \end{aligned} \quad (22)$$

and the momentum field

$$\begin{aligned} p_{i,l}\left(t + \frac{3\Delta t}{2}\right) - p_{i,l}\left(t + \frac{\Delta t}{2}\right) &= - \int_{t+\frac{1}{2}\Delta t}^{t+\frac{3}{2}\Delta t} dt' \frac{\partial \mathcal{H}(x, t' + \Delta t)}{\partial x_{i,l}} \\ &= - \frac{\partial \mathcal{H}(x, t + \Delta t)}{\partial x_{i,l}} \Delta t + \mathcal{O}(\Delta t^3) \end{aligned} \quad (23)$$

until we reach the stopping time, for example $1/\Delta t$. The Leapfrog method, as well as the conjugate gradient method (see below) have some systematical errors. To ensure their controllability at the end of each Leapfrog run we perform a Metropolis check to decide if we accept or reject the new auxiliary field configuration. It turns out that the acceptance depends on the size of the artificial Leapfrog time steps Δt as well as on the accuracy of the conjugate gradient method as studied in Ref. 27. Our experience tells us, that configurations will be rejected if the system is in a point of the phase space where the product of the gradient of the potential times the velocity in the according direction is large, compared to the artificial time steps. Therefore a second Leapfrog run with the same auxiliary field configuration but different initial momentum field may have much better propensity to produce a new configuration that will be accepted. If several Leapfrog runs fail, the time steps have to be made smaller.

We also implemented an adaptive Leapfrog method⁴⁰ that is also time reversible but selects the step-size according to the gradient of the Hamiltonian, $\Delta t \propto 1/|\nabla H|^2$. Summarizing, the acceptance is very good, but if a single bad conditioned configuration occurs, it slows down to very small time steps by trying to solve the equations of motions in regions of high variability and needs a very long time. These regions very likely correspond to regions discussed in Subsection IIF where the determinants change signs and therefore the symplectic integrator has tried to accommodate for the singularity in the gradient. Leapfrogs with fixed step size may fail at this configuration for several times, but after several runs with different momentum configurations they also will find a configuration that will be accepted, if the selected time step is not too large. Another way, we observed, to improve the acceptance is to substitute a Leapfrog run by several shorter runs. This generates the side effect of reduced correlations between measurements in some cases. We attribute this behavior to the additional generation of random ϕ_σ and p_σ fields between measurements. For larger system sizes or higher values of β it can be necessary to shorten the time steps Δt to keep the acceptance high.

D. Evaluation of the forces and measurement of observables

The evaluation of derivative, which are necessary to calculate the forces during the Leapfrog simulation, is simplified by using an algebraic identity as well as the symmetry of $M_\sigma^T M_\sigma$ to obtain

$$\frac{\partial}{\partial x_{i,l}} \phi_\sigma^T (M_\sigma^T(x) M_\sigma(x))^{-1} \phi_\sigma = -2 \phi_\sigma^T (M_\sigma^T(x) M_\sigma(x))^{-1} \left[M_\sigma^T(x) \left(\frac{\partial}{\partial x_{i,l}} M_\sigma(x) \right) \right] (M_\sigma^T(x) M_\sigma(x))^{-1} \phi_\sigma. \quad (24)$$

Measurements can be performed for every new configuration of the auxiliary fields. The bare one particle Green's function is given by the inverse M_σ matrix. Instead of a, numerically expensive, inversion of M_σ , every component $(M_\sigma^{-1})_{i,j}$ can be sampled by using $2[(M_\sigma^T M_\sigma)^{-1} \phi_\sigma]_i [R_\sigma]_j$ as an unbiased estimator. Wick's theorem allows to calculate also many particle observables. An efficient method for dealing with the linear system

$$M_\sigma^T M_\sigma X = \phi \quad (25)$$

and find the solution vector X is of utmost importance for an efficient implementation and is required for the sampling procedure in every Leapfrog step as well as for the measurement of observables. A more detailed discussion how to solve those systems of linear equations is discussed in the next subsection.

E. Solution of linear systems with the conjugate gradient method

In favor of readability we will suppress the spin index σ in this subsection, since the spin up and spin down sectors are treated in exactly the same way. As is well known, the straight-forward inversion of an $N \times N$ matrix by basic gaussian elimination needs $\mathcal{O}(N^3)$ flops. As mentioned above, we only need to know the solution of the linear system (25) to formulate the complete algorithm. In contrast to the inversion of a matrix, iteratively finding the solution to a system of linear equations up to the computing precision can be possible in an amount of computing time that is linear in the entries of the matrix and hence we can benefit greatly, if the system has a sparse system matrix. The workhorse method for symmetric, linear systems is the conjugate gradient (CG) method which we will explain on the basis of the prototypical system

$$OX = \phi. \quad (26)$$

The matrix $O = M^T M$, is symmetric and positive semi-definite. The solution to Eq. (26) can be interpreted as the unique minimum of the quadratic function

$$f(X) = \frac{1}{2} X^T O X - X^T \phi. \quad (27)$$

Given a starting guess X_0 , the idea is now not to take the direct gradient evaluated at each step but to choose search directions that are orthogonal, with respect to the from O induced scalar product, to all previously constructed directions. Employing that idea the following

iterative prescription emerges.

$$\begin{aligned} X_{n+1} &= X_n + \zeta_n d_n \\ r_{n+1} &= r_n - \zeta_n O d_n \\ \eta_n &= \langle r_{n+1}, r_{n+1} \rangle / \langle r_n, r_n \rangle \\ d_{n+1} &= r_{n+1} + \eta_n d_n \\ \zeta_{n+1} &= \langle r_{n+1}, r_{n+1} \rangle / \langle d_{n+1}, O d_{n+1} \rangle \end{aligned} \quad (28)$$

with iterative approximations X_n to the true solution X . We define the residual after the n th iteration by

$$r_n = \phi - O X_n. \quad (29)$$

The absolute value of the residual vector is something like a measure of how close the approximated solution is to the exact solution. Therefore, we use it to define a termination criterion for the iterative conjugate gradient method

$$\varepsilon_n = \sqrt{\frac{(\phi - O X_n)^2}{\phi^2}} \leq 10^{-7}, \quad (30)$$

similar to the criterion chosen in Ref. 25. The notation $\langle r, d \rangle$ represents a scalar product between two vectors r and d . To start the iterative procedure we have to choose an initial vector X_0 . If nothing is known about the system of equations it can be any arbitrary vector, like a vector consisting of zeros. A well designed guess can speed up the method and lower the number of iterations until it converges. Given X_0 the initial data is completed by

$$\begin{aligned} r_0 &= \phi - O X_0 \\ d_0 &= r_0. \end{aligned} \quad (31)$$

In general, it is possible to show, that

$$\langle d_m, O d_n \rangle = 0 \quad \text{for } m \neq n. \quad (32)$$

Therefore, all d_n vectors are linearly independent, with respect to O , and a calculation with exact arithmetic would deliver the exact result after N iterations. Like the authors of Ref. 25 mention, it is very common to speed up a conjugate gradient algorithm by introducing a preconditioner. It helps especially if the matrix is ill conditioned, which is known to be the case for stronger interaction strengths U and larger values of β^{41} . To define a suitable preconditioner we need a matrix \tilde{O} that is close to the matrix, representing the system of linear equations, but easy to invert. Because the matrix O is symmetric and positive semi definite, a good starting point is to use the Cholesky decomposition of O ,

$$\tilde{O} = L^T L. \quad (33)$$

The matrix L is a triangular matrix and thus easy to invert. We rewrite Eq. (26)

$$O'X' = \phi', \quad (34)$$

and we substitute

$$\begin{aligned} O' &= L^{-T}OL^{-1} \\ X' &= LX \\ \phi' &= L^{-T}\phi, \end{aligned} \quad (35)$$

from which it follows that

$$r'_n = \phi' - O'X'_n = L^{-T}r_n. \quad (36)$$

According to its definition, O' is also a symmetric and positive semi definite matrix. Therefore, we can apply the conjugate gradient method to Eq. (34) to solve the

modified system of linear equations. If we modify the iteration scheme, we get X out of

$$\begin{aligned} X_{n+1} &= X_n + \zeta'_n d_n \\ r_{n+1} &= r_n - \zeta'_n O d_n \\ \eta'_n &= \langle r_{n+1}, \tilde{O}^{-1} r_{n+1} \rangle / \langle r_n, \tilde{O}^{-1} r_n \rangle \\ d_{n+1} &= r_{n+1} + \eta'_n d_n \\ \zeta'_{n+1} &= \langle r_{n+1}, \tilde{O}^{-1} r_{n+1} \rangle / \langle d_{n+1}, O d_{n+1} \rangle. \end{aligned} \quad (37)$$

Once again, the numerical effort denies us the use of a usual Cholesky decomposition. Its exact calculation would be equivalent to the inversion of the matrix O . Instead, Ref. 25 proposes an incomplete Cholesky decomposition. They use the matrix product $M^T M$, without hopping interactions and a slight shift of the diagonal elements. The matrix we decompose is given by the matrix of Eq. (38).

$$\tilde{O}_0 = \begin{pmatrix} \alpha I + B_{0,1}^2 & -B_{0,1} & 0 & \cdots & 0 & B_{0,N_\tau} \\ -B_{0,1} & \alpha I + B_{0,2}^2 & -B_{0,2} & \cdots & 0 & 0 \\ 0 & -B_{0,2} & \alpha I + B_{0,3}^2 & \cdots & 0 & 0 \\ \vdots & \vdots & \vdots & \ddots & \vdots & \vdots \\ 0 & 0 & 0 & \cdots & \alpha I + B_{0,N_\tau-1}^2 & -B_{0,N_\tau-1} \\ B_{0,N_\tau} & 0 & 0 & \cdots & -B_{0,N_\tau-1} & \alpha I + B_{0,N_\tau}^2 \end{pmatrix} \quad (38)$$

All block matrices $B_{0,i}$ are now diagonal. The slight shift, e.g. $\alpha = 1.05$, prevents the matrix to become ill conditioned and prevents a pivot breakdown of the CG⁴². The matrix defined in Eq. (38) can not be inverted analytically for $\alpha \neq 1$ ²⁵. The new preconditioner matrix is given by

$$\tilde{O}' = L^T D L. \quad (39)$$

With diagonal matrix

$$D = \begin{pmatrix} D_1 & 0 & 0 & \cdots & 0 & 0 \\ 0 & D_2 & 0 & \cdots & 0 & 0 \\ 0 & 0 & D_3 & \cdots & 0 & 0 \\ \vdots & \vdots & \vdots & \ddots & \vdots & \vdots \\ 0 & 0 & 0 & \cdots & D_{N_\tau-1} & 0 \\ 0 & 0 & 0 & \cdots & 0 & D_{N_\tau} \end{pmatrix}, \quad (40)$$

as well as the triangular matrices

$$L = \begin{pmatrix} I & -L_1 & 0 & \cdots & 0 & L_{N_\tau} \\ 0 & I & -L_2 & \cdots & 0 & 0 \\ 0 & 0 & I & \cdots & 0 & 0 \\ \vdots & \vdots & \vdots & \ddots & \vdots & \vdots \\ 0 & 0 & 0 & \cdots & I & -L_{N_\tau-1} \\ 0 & 0 & 0 & \cdots & 0 & I \end{pmatrix}. \quad (41)$$

In the atomic limit now all of them consist of diagonal block matrices of size $V_S \times V_S$. Recursive definitions of

those matrices keep the numerical effort down. The matrices for $l = 1, \dots, N_\tau - 1$ are given by

$$\begin{aligned} L_l &= D_l^{-1} B_{0,l} \\ D_l &= \alpha I + B_{0,l}^2 - B_{0,l-1} D_{l-1}^{-1} B_{0,l-1}, \end{aligned} \quad (42)$$

while for $l = N_\tau$

$$\begin{aligned} L_{N_\tau} &= D_1 B_{0,N_\tau} \\ D_{N_\tau} &= \alpha I + B_{0,N_\tau}^2 - B_{0,N_\tau-1} D_{N_\tau-1}^{-1} B_{0,N_\tau-1} \\ &\quad - B_{0,N_\tau} D_1^{-1} B_{0,N_\tau} \end{aligned} \quad (43)$$

With these preliminaries the preconditioned conjugate gradient method can be used as described above. One could ask the question, if the preconditioner we use is a good choice for our purposes. It is not easy to answer this question precisely. We are following the arguments of Scalettar et al. in Ref. 25, where they are proposing that the condition of the matrix, and thus the number of conjugate gradient iterations, depends essentially on the interaction strength U . The search for a better preconditioner is still ongoing and the only progress we know of can be found in Ref. 42, where progress for very strong interactions is reported, although we like to point out that their tests were not performed on real configurations from a full Monte Carlo simulation but on randomly generated configurations of the auxiliary field. The preconditioner, we have chosen, is well suited for interactions

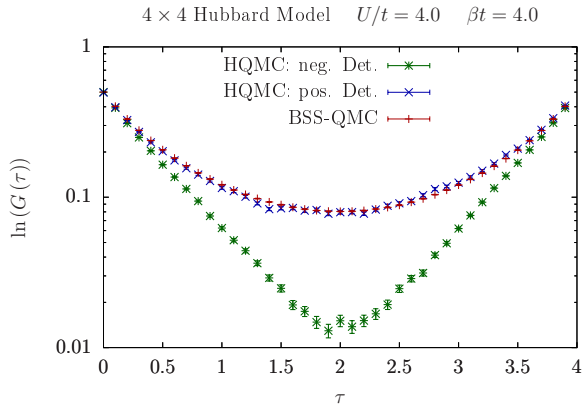


FIG. 1. Green's functions, calculated with the Hybrid Quantum Monte Carlo and the BSS-QMC³⁰ algorithms on a 4×4 -lattice at $U = 4$ and $\Delta_\tau = 0.1$. Starting the simulation in different sectors clearly produces different results.

that are not too strong and especially fast to calculate because of the sparsity structure of our matrix. Nevertheless even the preconditioned system can come to a configuration where the CG method never reaches the claimed accuracy; hence we will stop it after N iterations and take the solution vector of this iteration or the one with the smallest deviation. In general this problem occurs only for simulations with very inappropriate parameters and can be absorbed in the considerations of acceptance rates below.

F. Ergodicity issues

The implementation described until now, was already discussed in the original paper²⁵. We were able to reimplement the method and run it with several lattice configurations. Furthermore we also observed that for small values of β , the configuration space is strongly dominated by configurations where both determinants are positive and hence the Monte Carlo process encounters no difficulties in sampling this wide space. If we increase the inverse temperature, the configuration space becomes much more fissured into $(+, +)$ ($\text{sign det}(M_\sigma) = 1$) and $(-, -)$ ($\text{sign det}(M_\sigma) = -1$) domains. Since the determinants are real continuous functions of a continuous field, $(+, +)$ and $(-, -)$ domains are necessarily separated by regions where $(M_\sigma^T M_\sigma)^{-1}$ diverges.

This clearly poses a problem, since any implementation of Molecular Dynamics with symplectic integrators conserves energy and will in principle never cross such a barrier⁴³. In particular, every Molecular Dynamics run will be trapped in the pocket of the configuration space where it started. Since the simple sampling of the momenta and pseudo-fermion fields does not allow to cross the barriers, a Monte Carlo run will not be ergodic and

can converge to wrong result as demonstrated in Fig. 1. The figure demonstrates that starting a run in a $(+, +)$ or $(-, -)$ domain indeed leads to different results.

The behavior of different integrators is quite interesting close to those boundaries. If we use the simple Leapfrog with large step sizes, it is able to cross over into other domains, by violating energy conservation. The adaptive integrator⁴⁰ on the other hand will in this setting dutifully correct its step size down to vanishingly small values to accommodate for the large gradient of the potential that it tries to sample. It will not cross the boundary but it will slow down the simulation indefinitely while trying to integrate the equations of motion with and preserving the total energy conservation.

III. COMPLEX REFORMULATION AND COMPARISON

One can follow several routes to circumvent the ergodicity issues of the algorithm using real auxiliary fields. On one hand one could try to eliminate the potential barriers in configuration space by a suitable transformation of the problem. Another idea is to modify the Leapfrog so that it can explicitly tunnel between the barriers⁴³. Here we will follow the idea of extending the configuration space to complex numbers²⁹.

A. Complexification

In a complex configuration space the barriers still exist but, due to the additional degrees of freedom, the integrator should be able to produce trajectories that move around them. The determinants become complex numbers and are conjugate to each other, thereby ensuring the absence of negative sign problem. To achieve this complexification, we decouple the Hubbard interaction in charge and spin sectors by introducing a free parameter α :

$$H'_V = \sum_i \alpha \frac{U}{2} (\hat{n}_{i,\uparrow} + \hat{n}_{i,\downarrow} - 1)^2 - \sum_i (1 - \alpha) \frac{U}{2} (\hat{n}_{i,\uparrow} - \hat{n}_{i,\downarrow})^2. \quad (44)$$

α can be chosen from $[0, 1]$ thereby interpolating between the purely real code at $\alpha = 0$ and a purely imaginary one at $\alpha = 1$. Clearly the final result will be α -independent, but it will determine the Monte Carlo configuration space. In this section, we will redefine some of the symbols, variables and matrices that we have introduced previously. To distinguish between the original and the new definitions, all redefined variables will be labeled by a prime. The new formulation leads to a doubling of auxiliary fields:

$$e^{-\Delta_\tau H'_U} \propto \int dx_{i,l} dy_{i,l} \exp \left\{ -\Delta_\tau \sum_i \left[x_{i,l}^2 + y_{i,l}^2 + \left(\sqrt{2U(1-\alpha)} x_{i,l} + i\sqrt{2U\alpha} y_{i,l} \right) \left(\hat{n}_{i,\uparrow} - \frac{1}{2} \right) - \left(\sqrt{2U(1-\alpha)} x_{i,l} - i\sqrt{2U\alpha} y_{i,l} \right) \left(\hat{n}_{i,\downarrow} - \frac{1}{2} \right) \right] \right\}, \quad (45)$$

and we also redefine

$$S'_B(x, y) := \Delta_\tau \sum_i (x_i^2 + y_i^2). \quad (46)$$

To shorten the notation, we will sometimes use a combined notation and interpret both auxiliary fields as components of one complex field

$$z_{i,l} := \sqrt{2U(1-\alpha)} x_{i,l} + i\sqrt{2U\alpha} y_{i,l}. \quad (47)$$

We formulate the partition function for complex auxiliary fields similar to the real case

$$Z = \int [\delta z \delta \bar{z}] e^{-S_B(z, \bar{z})} e^{\Delta_\tau \sum_{i,l} z_{i,l}/2} \det M'_\uparrow(z, \bar{z}) \times e^{-\Delta_\tau \sum_{i,l} \bar{z}_{i,l}/2} \det M'_\downarrow(z, \bar{z}). \quad (48)$$

The matrices for the spin up and spin down sector still have the same structure as before

$$M'_\sigma = \begin{pmatrix} I & 0 & 0 & \cdots & 0 & B'_{N_\tau, \sigma} \\ -B'_{1, \sigma} & I & 0 & \cdots & 0 & 0 \\ 0 & -B'_{2, \sigma} & I & \cdots & 0 & 0 \\ \vdots & \vdots & \vdots & \ddots & \vdots & \vdots \\ 0 & 0 & 0 & \cdots & I & 0 \\ 0 & 0 & 0 & \cdots & -B'_{N_\tau-1, \sigma} & I \end{pmatrix}, \quad (49)$$

with

$$B'_{l, \sigma}(z, \bar{z}) = e^{-\Delta_\tau K} e^{-\sigma \Delta_\tau V'_{l, \sigma}(z, \bar{z})}, \quad (50)$$

and

$$(V'_{l, \sigma})_{i,j}(z, \bar{z}) = \begin{cases} z_{i,l} \delta_{i,j} & \sigma = \uparrow \\ \bar{z}_{i,l} \delta_{i,j} & \sigma = \downarrow \end{cases}. \quad (51)$$

At half filling, particle-hole symmetry induces a relation between the determinants of the spin matrices and their prefactors

$$e^{-\Delta_\tau \sum_{i,l} \frac{\bar{z}_{i,l}}{2}} \det M'_\downarrow = \overline{e^{\Delta_\tau \sum_{i,l} \frac{z_{i,l}}{2}} \det M'_\uparrow} = e^{\Delta_\tau \sum_{i,l} \frac{\bar{z}_{i,l}}{2}} \det M'^{\dagger}_\uparrow. \quad (52)$$

This means, that the statistical weight for every configuration is positive such that complexification does not lead to a sign problem. Furthermore, we can use this relation

to simplify the algorithm by substituting the spin down sector by the complex conjugate of the spin up sector

$$Z = \int [\delta z \delta \bar{z}] e^{-S'_B(z, \bar{z})} e^{\Delta_\tau \sum_{i,l} \frac{z_{i,l} + \bar{z}_{i,l}}{2}} \times \det M'_\uparrow(z, \bar{z}) \det M'^{\dagger}_\uparrow(z, \bar{z}) \\ = \int [\delta x \delta y] e^{-S'_B(x, y)} \det \left[e^{\Delta_\tau \frac{\sqrt{2U(1-\alpha)}}{N_\tau V_S} \sum_{i,l} x_{i,l}} \times M'_\uparrow(x, y) M'^{\dagger}_\uparrow(x, y) \right] \\ = \int [\delta x \delta y] e^{-S'_B(x, y)} \det [\mathcal{M}_\uparrow(x, y) \mathcal{M}_\uparrow^\dagger(x, y)]. \quad (53)$$

Here we defined

$$\mathcal{M}_\uparrow(x, y) := \kappa(x) M'_\uparrow(x, y) \quad (54)$$

and

$$\kappa(x) := \exp \left\{ \Delta_\tau \frac{\sqrt{2U(1-\alpha)}}{2N_\tau V_S} \sum_{i,l} x_{i,l} \right\}. \quad (55)$$

As in section II, the determinants can be eliminated by the use of a gaussian identity, which introduces additional complex fields

$$Z = \int [\delta x \delta y \delta \phi'_\uparrow \delta \phi'^{\dagger}_\uparrow] e^{-S'_B - \phi'^{\dagger}_\uparrow (\mathcal{M}_\uparrow^\dagger \mathcal{M}_\uparrow)^{-1} \phi'_\uparrow}. \quad (56)$$

The partition function is now comparable in its form to the previous real algorithm. Instead of a real system of linear equations we now have to solve a complex one. Although the number of degrees of freedom is twice as large, we can use a complex version of the conjugate gradient method. Since we eliminated the spin down sector in the formulation, we get away with one call to the CG method. The sampling of random numbers works analogously to the real version of the algorithm. We redefine

$$R'_\sigma := (\mathcal{M}_\sigma^T(x, y))^{-1} \phi'_\sigma \Rightarrow Z \propto e^{-R'^{\dagger}_\sigma R'_\sigma}, \quad (57)$$

and generate gaussian random numbers for the real and imaginary part of R'_σ and perform a matrix vector multiplication to get the complex ϕ'_σ fields

$$\phi'_\sigma = \mathcal{M}_\sigma^\dagger(x, y) R'_\sigma. \quad (58)$$

Since we doubled our auxiliary field components, we also have to introduce two momentum fields to get a new

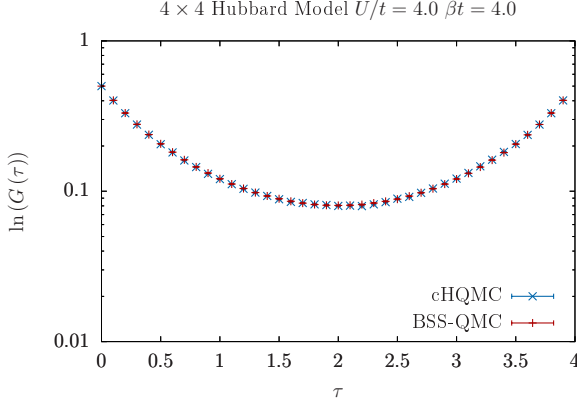


FIG. 2. Single particle Green's function, calculated with the complex HQMC algorithm and compared to the results of a BSS-QMC run³⁰ for the same parameters as Fig. 1.

artificial Hamiltonian

$$\begin{aligned} \mathcal{H}'(x, y, p_x, p_y, \phi'_\uparrow, \phi'^\dagger_\uparrow) := & \\ S'_B(x, y) + \sum_{i,l} \left((p_x)_{i,l}^2 + (p_y)_{i,l}^2 \right) + & \\ + \phi'^\dagger_\uparrow \left(\mathcal{M}'_\uparrow(x, y) \mathcal{M}_\uparrow(x, y) \right)^{-1} \phi'_\uparrow. & \end{aligned} \quad (59)$$

Both momentum fields are gaussian distributed and thereby easy to sample. Hamilton's equations of motion lead the way to the complex Leapfrog method.

$$\begin{aligned} \dot{x}_{i,l} &= \frac{\partial \mathcal{H}'(x, y)}{\partial (p_x)_{i,l}} = 2(p_x)_{i,l}, \\ \dot{y}_{i,l} &= \frac{\partial \mathcal{H}'(x, y)}{\partial (p_y)_{i,l}} = 2(p_y)_{i,l}, \end{aligned} \quad (60)$$

$$(\dot{p}_x)_{i,l} = -\frac{\partial \mathcal{H}'(x, y)}{\partial (x)_{i,l}}, \quad (\dot{p}_y)_{i,l} = -\frac{\partial \mathcal{H}'(x, y)}{\partial (y)_{i,l}}. \quad (61)$$

Since the equations of motion decouple for the two parts of the auxiliary field, we find that the complex version of the algorithm just leads to a doubling of the degrees of freedom. To measure the single particle Green's function we invert the M'_σ matrix stochastically and come to the unbiased estimator $[(M'^\dagger_\sigma M'_\sigma)^{-1} \phi_\sigma]_i [R'_\sigma]_j$ for $(M'^{-1}_\sigma)_{i,j}$. Since we are dealing with complex numbers, also the estimator will give complex estimates. In the process of averaging the observables over the Monte Carlo configurations their imaginary part has to vanish.

B. Results of the complex method

If we now recalculate the single particle Green's function with the same parameters, where the real version of the algorithm previously failed, we observe consistent

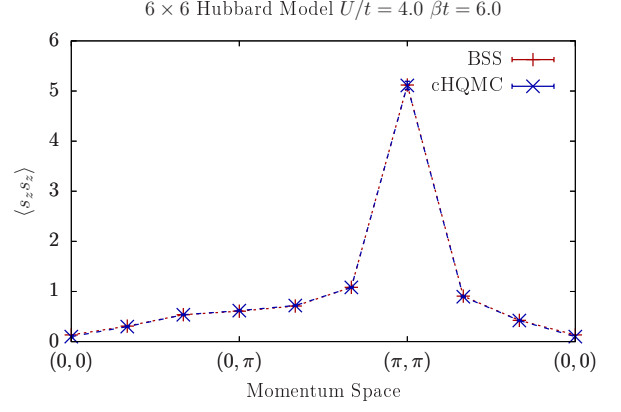


FIG. 3. HQMC results for the spin-spin-correlation functions in momentum space. Good agreement with benchmarks results from the BSS runs³⁰ is obtained.

results, as shown in Fig. 2. Beside the single particle Green's function we can also calculate higher observables like the spin-spin correlation function of a system, as shown in Fig. 3. Wick's theorem allows us to decompose many particle Green's functions into expressions involving only single particle Green's functions. Because we calculate the Green's functions only stochastically we get additional noise for many particle Green's functions and hence have to generate more samples.

To analyze the runtime of the algorithm we carried out simulations in one, two and three dimensions at different inverse temperatures. Generically, and contrary to our aspirations, the runtime does not seem to scale favorably with system size and inverse temperature. There are many reasons for this. The first is the observation that the number of iterations required for the conjugate gradient method to converge grows nearly linearly with the Euclidean size of the system. Another reason is that to keep the acceptance high, we have to rescale the artificial Leapfrog time step as $\Delta t \propto V_s^{-1} \beta^{-1}$. Combined with the linear scaling that every vector operation needs we achieved a scaling of approximately

$$(L^d \beta)^{2.5-3.0}. \quad (62)$$

C. Comparison between cHQM and BSS for the Hubbard model

Finally we have to compare the efficiency of the cHQM with other simulation techniques. The BSS-QMC method as implemented in the ALF software package³⁰ is a well established and optimized algorithm to simulate half-filled Hubbard systems at finite temperature. Both methods have the same, Trotter-decomposition induced, systematic error which predetermines them for a comparison. Besides properties such as

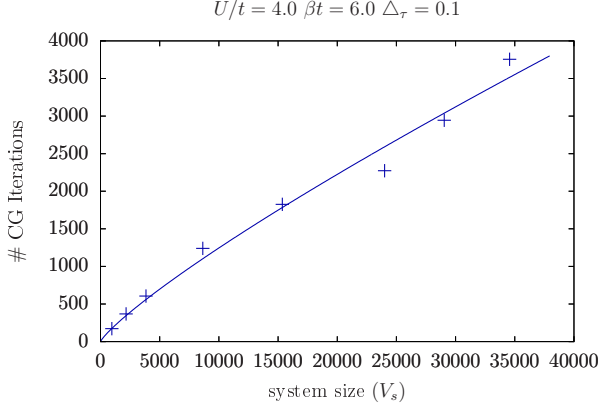


FIG. 4. Average number of CG iterations needed, to solve a system of linear equations, as a function of the Euclidean system size as given by the number of Trotter slices times the lattice size ($N_\tau V_s$). For a two dimensional system at fixed temperature, the plot shows an approximately linear behavior as function of the lattice size.

required memory and effective scaling for a single step, fluctuations due to the statistical nature of the approach is a key property of every Monte Carlo method. Owing to the central limit theorem, error-bars decrease as the square root of the number of measured samples, i.e. computing time. Fluctuations correspond to the prefactor of this behavior. Fig. 5 shows the decay of stochastic errors for both methods for several system sizes. Both methods show the expected behavior as a function of computational time. However, for given computational time, the BSS method achieves much higher precision than the cHQMC. For this comparison we have carefully chosen the parameter set. It is known that the spin correlation length of the half-filled Hubbard model grows exponentially with inverse temperature. The temperature regime where this scaling is valid corresponds to the so-called renormalized classical regime⁴⁴. Our choice of parameters, $U/t = 4$ and $\beta t = 6$ places us in this regime²⁰, which can be considered as *hard* for Monte Carlo simulations.

IV. HQMC AND THE SSH MODEL

The question we would like to pose in this section is if there exists a class of models in the solid state where the HQMC is the method of choice. We will argue that the Su-Schrieffer-Heeger (SSH) model³¹ describing the electron-phonon problem could lie in this class. An obvious difficulty for the HQMC method are singularities in the effective action trigger by the sign change of the determinant in a given spin sector. Using a Majorana representation, one will show that the determinant in a given spin sector is always positive semi-definite for the SSH model at the particle-hole symmetric point. Furthermore, other Monte Carlo methods face issues for this electron-phonon problem. In the CT-INT approach^{32–34}

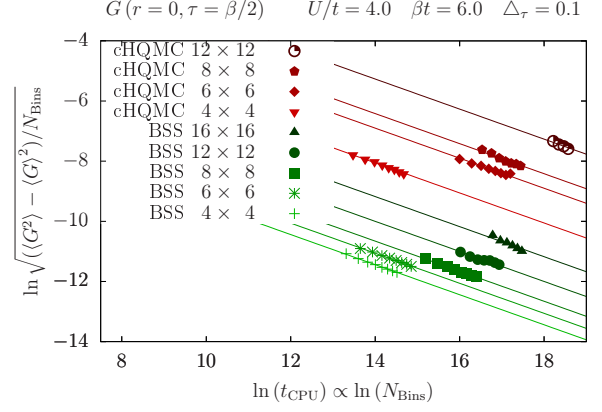


FIG. 5. Comparison of the BSS and cHQMC. Here we compare errorbars σ as function of computing time for several system sizes.

the phonon degrees of freedom are integrated out but in spacial dimensions larger than unity and away from the anti-adiabatic limit this generates a negative sign problem. In the BSS algorithm where phonons degrees of freedom are sampled, one can foresee that local moves will lead to large autocorrelation times³⁵ such that global updating schemes such as Langevin dynamics or Hybrid Monte Carlo should perform better.

A. HQMC formulation for the SSH model

The SSH Hamiltonian is given by,

$$\hat{H} = \hat{H}_{\text{el}} + \hat{H}_{\text{ph}} + \hat{H}_{\text{ep}}. \quad (63)$$

Here,

$$\hat{H}_{\text{el}} = -t \sum_{\langle i,j \rangle, \sigma} \left(\hat{c}_{i,\sigma}^\dagger \hat{c}_{j,\sigma} + \hat{c}_{j,\sigma}^\dagger \hat{c}_{i,\sigma} \right), \quad (64)$$

is the kinetic energy and $\langle i,j \rangle$ denotes the nearest neighbors of a square lattice. Harmonic oscillators on links account for the lattice vibrations,

$$\hat{H}_{\text{ph}} = \sum_{\langle i,j \rangle} \left[\frac{\hat{P}_{\langle i,j \rangle}^2}{2m} + \frac{k}{2} \hat{Q}_{\langle i,j \rangle}^2 \right], \quad (65)$$

with \hat{P}, \hat{Q} being the conjugate momentum and position operators. The electron-phonon coupling leads to a modulation of the hopping matrix element:

$$\hat{H}_{\text{ep}} = g \sum_{\langle i,j \rangle, \sigma} \hat{Q}_{\langle i,j \rangle} \left(\hat{c}_{i,\sigma}^\dagger \hat{c}_{j,\sigma} + \hat{c}_{j,\sigma}^\dagger \hat{c}_{i,\sigma} \right) \quad (66)$$

with a coupling strength g . To simplify the notation we label bond indices as

$$b := \langle i,j \rangle, \quad (67)$$

and introduce the bond hopping as

$$\hat{K}_b := \left(\hat{c}_i^\dagger \hat{c}_j + \hat{c}_j^\dagger \hat{c}_i \right). \quad (68)$$

To formulate the path integral, we will chose a real space basis:

$$\hat{Q}_b |x_b\rangle = x_b |x_b\rangle, \quad (69)$$

such that the partition function reads,

$$Z = \text{Tr} \int \prod_b dx_b \langle x_b | e^{-\beta \hat{H}} | x_b \rangle, \quad (70)$$

where the trace runs over the fermionic degrees of freedom. The standard real space path integral and integration over the fermionic degrees of freedom yields the result:

$$Z = \int \prod_{b,\tau} dx_{b,\tau} e^{-S_0(x)} [\det M(x)]^{N_{\text{col}}}, \quad (71)$$

which is similar to the representation of the Hubbard model in Eq. (6). Being a phonon field, as opposed to a Hubbard-Stratonovich one, $x_{b,\tau}$ has a bare imaginary time dynamics given by the action

$$S_0(x) := \Delta_\tau \sum_{b,\tau} \left(\frac{m}{2} \left[\frac{x_{b,\tau+1} - x_{b,\tau}}{\Delta_\tau} \right]^2 + \frac{k}{2} x_{b,\tau}^2 \right), \quad (72)$$

of the harmonic oscillator. In the above, we have considered a model with N_{col} spin components corresponding to an $\text{SU}(N_{\text{col}})$ symmetric model. The $M(x)$ matrix has the same block structure as in Eq. (8) with

$$B_\tau = \exp \left\{ -\Delta_\tau \sum_b (gx_{b,\tau} - t) K_b \right\}. \quad (73)$$

To show the absence of singularities in the action one should demonstrate that $\det M(x) > C$ with C a finite

positive constant. Here we can only show a weaker statement, namely that $\det M(x) \geq 0 \forall x$. Considering only one color degree of freedom, and the Majorana representation on sublattices A and B ,

$$\begin{aligned} i \in A: \quad & \hat{\gamma}_{i,1} = \left(\hat{c}_i + \hat{c}_i^\dagger \right) & \hat{\gamma}_{i,2} = -i \left(\hat{c}_i - \hat{c}_i^\dagger \right) \\ i \in B: \quad & \hat{\gamma}_{i,1} = -i \left(\hat{c}_i - \hat{c}_i^\dagger \right) & \hat{\gamma}_{i,2} = - \left(\hat{c}_i + \hat{c}_i^\dagger \right) \end{aligned} \quad (74)$$

the exponent in Eq. (73) reads

$$\begin{aligned} \sum_b (-t + gx_{b,\tau}) \left(\hat{c}_i^\dagger \hat{c}_j + \hat{c}_j^\dagger \hat{c}_i \right) \\ = \frac{i}{2} \sum_{b,n} (-t + gx_{b,\tau}) \hat{\gamma}_{i,n} \hat{\gamma}_{j,n}. \end{aligned} \quad (75)$$

The above result depends upon the fact that the hopping matrix element is real, and that hopping occurs only between different sublattices. Thereby, the trace factorizes

$$\begin{aligned} \text{Tr} \prod_{\tau=1}^{N_\tau} e^{-\Delta_\tau \sum_b (-t + gx_{b,\tau}) (\hat{c}_i^\dagger \hat{c}_j + \hat{c}_j^\dagger \hat{c}_i)} \\ = \left[\text{Tr} \prod_{\tau=1}^{N_\tau} e^{-i \frac{\Delta_\tau}{4} \sum_b (-t + gx_{b,\tau}) \hat{\gamma}_i \hat{\gamma}_j} \right]^2. \end{aligned} \quad (76)$$

and one can show that the trace over a one Majorana mode is a real quantity². Thereby, $\det M(x) \geq 0 \forall x$.

Going on to implement a HQMC method for the SSH model, we define

$$\tilde{x}_{b,\tau} := \sqrt{\frac{k}{2}} x_{b,\tau} \quad \omega_0^2 := \frac{k}{m} \quad \tilde{g} := \sqrt{\frac{2}{k}} g. \quad (77)$$

and include the canonical conjugate momentum and pseudo fermions to obtain:

$$Z = \int [\delta x \delta p \delta \phi_\sigma] \exp \left\{ -\Delta_\tau \underbrace{\left[\sum_b \left(\omega_0^{-2} \left[\frac{\tilde{x}_{b,\tau+1} - \tilde{x}_{b,\tau}}{\Delta_\tau} \right]^2 + \tilde{x}_{b,\tau}^2 \right) \right]}_{=S_0(\tilde{x})} - \sum_{\sigma=N_{\text{col}}} \phi_\sigma^\text{T} (M^\text{T} M)^{-1} \phi_\sigma - \sum_b p_{b,\tau}^2 \right\} \quad (78)$$

Henceforth, everything is similar to implementation for the Hubbard model. After generating random numbers for p and ϕ_σ fields a Leapfrog run updates the auxiliary field, followed by measurements of observables before the loop starts again. A CG method is put to use to solve the system of linear equations.

B. Proof of Concept

In Fig. 6 and Fig. 7 our HQMC results for the SSH model are benchmarked against CT-INT simulations in a regime where the latter method does not suffer from a severe sign problem. As apparent, perfect agreement is obtained.

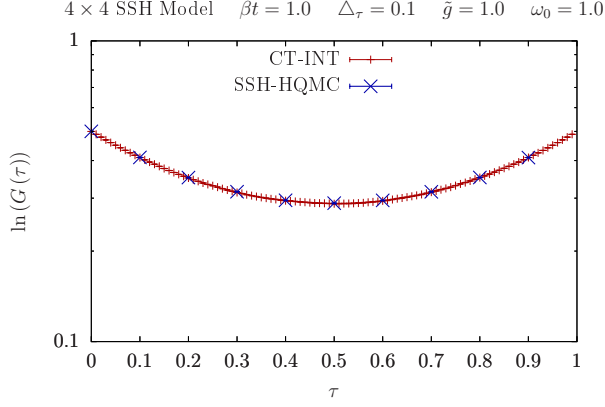


FIG. 6. HQMC and CT-INT results for the local Green function for SSH model.

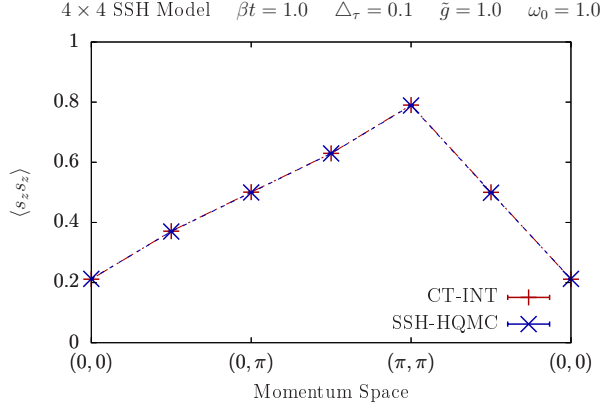


FIG. 7. HQMC and CT-INT spin-spin correlation functions in the momentum space for the SSH model.

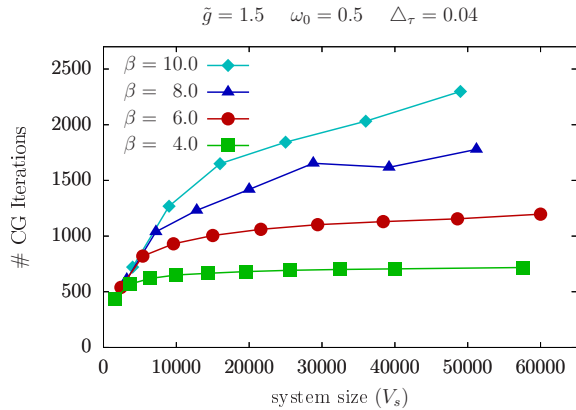


FIG. 8. Number of CG iterations required for a given accuracy as functions of the lattice size at various temperatures. At each temperature one can observe saturation. The lattice size at which this saturation kicks in is temperature dependent. Here we considered 4×4 , 6×6 , 8×8 , 10×10 , 12×12 , 14×14 , 18×18 , 20×20 and 24×24 lattices.

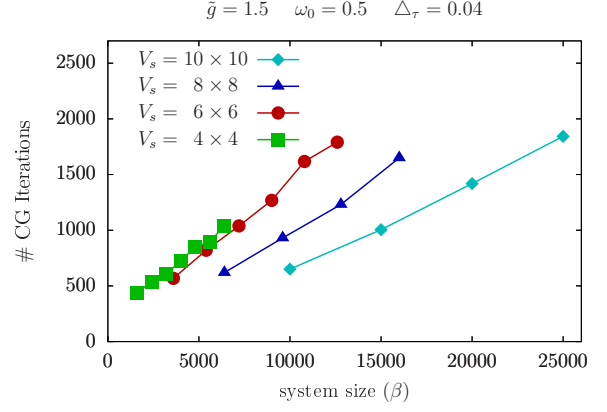


FIG. 9. Number CG iterations as a function of inverse temperature at different lattice sizes. In this case, no saturation is observed in the considered temperature range. Here we consider $\beta = 4.0, 6.0, 8.0$ and 10.0 .

The scaling behavior of the HQMC method for the SSH model seems more favorable than for the Hubbard model. We observe a much weaker dependence of the acceptance on the Leapfrog step size. For the SSH model a correction of approximately $\Delta t \propto V_s^{-0.25} \beta^{-0.25}$ was sufficient in most cases. Note that for the Hubbard model, the time step had to be scaled as $\Delta t \propto V_s^{-1} \beta^{-1}$. We believe that this reflects the fact that singularities in the effective action are not an issue.

Fig. 8 and Fig. 9 plot the number of CG steps required during the simulation so as to achieve the desired accuracy. This result, alongside the favorable Leapfrog step scaling, gives an estimate of the numerical effort:

$$(L^d)^{1.25-1.5} \beta^{2.25-2.5}. \quad (79)$$

It is interesting to note the asymmetry in the temporal and spatial directions (see Figs. 8 and 9). A possible understanding of this is in terms of a dynamical exponent greater than unity that renders the characteristic length scales longer along the imaginary time than in real space.

V. CONCLUSION

By design, the HQMC algorithm has the potential of solving sign free fermion problems with a numerical effort scaling linearly with the Euclidean system size, $V_s \beta$. The key ideas leading to this statement are the following.

- Stochastic sampling of the fermion determinant.
- Global molecular dynamics updating schemes.
- Stochastic sampling of the single particle Green functions required for the computation of observables.

Remarkably the above relies solely on the solution of Eq. 26, $M^T M X = \phi$, and since M contains only order $V_s \beta$ non-vanishing matrix elements one can hope for linear scaling in $V_s \beta$.

For the Hubbard model at half-filling, the major issue are the zeros of determinant of the fermion matrix M . Even though the total weight is positive, the sign of the determinant in a single spin sector at *low* temperatures fluctuates strongly. We showed that this leads to ergodicity issues since the zeros split the configuration space in regions separated by infinite potential barriers that cannot be overcome with molecular dynamics. To circumvent this problem we have complexified the Hubbard-Stratonovich transformation so as to be able to *go around* these singularities. Our main result, however, is that in comparison to the generic BSS algorithm as implemented in the ALF project³⁰, the complexified HQMC for the Hubbard model remains orders of magnitude slower. This statement relies on the following observations. i) Fluctuations of standard observables are much larger. ii) The roughness of the potential landscape renders an efficient implementation of the molecular dynamics challenging. In other words, the forces are hard to compute and the CG approach fails to converge in a number of iterations that scale with the Euclidean volume. These statements are based on a simple implementation of the HQMC, and much progress has been made to solve the above issues by for instance sampling the n th root of the fermion matrix^{45,46}.

Since the sign changes of the fermion determinant in a given spin sector render the implementation of the HQMC hard, one will invariably search for interesting models where the determinant remains positive for all field configurations. Using recent insights from the Majorana representation² to classify sign free Hamiltonians, one will show that the SSH model on a bipartite lattice at half-filling falls in this class. This model describes the

salient physics of the electron-phonon interaction, and is solvable in one dimension with the CT-INT approach⁴⁷. In higher dimensions, its phase diagram remains illusive: a simple sign free implementation of the BSS will suffer from long autocorrelation times whereas the CT-INT approach in which the phonons are integrated out turns out to suffer from a sign problem away from the anti-adiabatic limit. Our preliminary results in solving this model with the HQMC are very promising. Away from half-filling and/or away from the particle-hole symmetric point, the model for an even number of fermion flavors does not suffer from the negative sign problem and can be simulated with the HQMC. In this case however, the sign of the determinant for a single flavor can start fluctuating and thereby reduce the efficiency of the HQMC. It is however unclear to what extent the efficiency of the algorithm will suffer away from the particle symmetric point. Further work in this direction is presently under progress.

ACKNOWLEDGMENTS

We are very indebted to Martin Hohenadler for providing the SSH test data and for fruitful discussions on numerous occasions. We acknowledge fruitful discussions with N. Brambilla, P. Buividovich, M. Hasenbusch, A. Kennedy, M. Körner, D. Schaich, L. Smekal, D. Smits, J. Thies from the ESSSEX project (<https://blogs.fau.de/essex/>), M. Ulybyshev, J. Weber, and finally KONWIHR (<http://www.konwihr.uni-erlangen.de>) for algorithmic support. The authors gratefully acknowledge the Gauss Centre for Supercomputing e.V. (www.gauss-centre.eu) for funding this project by providing computing time on the GCS Supercomputer SuperMUC at Leibniz Supercomputing Centre (LRZ, www.lrz.de). We thank the SFB 1170 “Tocotronics” for funding under the grant numbers C01 (FFA and SB) as well as Z03 (FG).

-
- ¹ C. Wu and S.-C. Zhang, Phys. Rev. B **71**, 155115 (2005).
 - ² Z.-X. Li, Y.-F. Jiang, and H. Yao, Phys. Rev. B **91**, 241117 (2015).
 - ³ Z.-X. Li, Y.-F. Jiang, and H. Yao, Phys. Rev. Lett. **117**, 267002 (2016).
 - ⁴ Z. C. Wei, C. Wu, Y. Li, S. Zhang, and T. Xiang, Phys. Rev. Lett. **116**, 250601 (2016).
 - ⁵ S. Capponi and F. F. Assaad, Phys. Rev. B **63**, 155114 (2001).
 - ⁶ F. F. Assaad, Phys. Rev. B **71**, 075103 (2005).
 - ⁷ M. Hohenadler, T. C. Lang, and F. F. Assaad, Phys. Rev. Lett. **106**, 100403 (2011).
 - ⁸ E. F. Huffman and S. Chandrasekharan, Phys. Rev. B **89**, 111101 (2014).
 - ⁹ L. Wang, P. Corboz, and M. Troyer, New Journal of Physics **16**, 103008 (2014).
 - ¹⁰ F. F. Assaad and T. Grover, Phys. Rev. X **6**, 041049 (2016).
 - ¹¹ S. Gazit, M. Randeria, and A. Vishwanath, Nat Phys **13**, 484 (2017).
 - ¹² F. F. Assaad and I. F. Herbut, Phys. Rev. X **3**, 031010 (2013).
 - ¹³ F. Parisen Toldin, M. Hohenadler, F. F. Assaad, and I. F. Herbut, Phys. Rev. B **91**, 165108 (2015).
 - ¹⁴ Y. Otsuka, S. Yunoki, and S. Sorella, Phys. Rev. X **6**, 011029 (2016).
 - ¹⁵ E. Berg, M. A. Metlitski, and S. Sachdev, Science **338**, 1606 (2012), <http://www.sciencemag.org/content/338/6114/1606.full.pdf>.
 - ¹⁶ Y. Schattner, S. Lederer, S. A. Kivelson, and E. Berg, Phys. Rev. X **6**, 031028 (2016).
 - ¹⁷ X. Y. Xu, K. Sun, Y. Schattner, E. Berg, and Z. Y. Meng, ArXiv e-prints (2016), arXiv:1612.06075 [cond-mat.str-el].
 - ¹⁸ T. Sato, M. Hohenadler, and F. F. Assaad, ArXiv e-prints (2017), arXiv:1707.03027 [cond-mat.str-el].
 - ¹⁹ R. Blankenbecler, D. J. Scalapino, and R. L. Sugar, Phys. Rev. D **24**, 2278 (1981).
 - ²⁰ S. White, D. Scalapino, R. Sugar, E. Loh, J. Gubernatis,

- and R. Scalettar, Phys. Rev. B **40**, 506 (1989).
- ²¹ F. Assaad and H. Evertz, in *Computational Many-Particle Physics*, Lecture Notes in Physics, Vol. 739, edited by H. Fehske, R. Schneider, and A. Weiße (Springer, Berlin Heidelberg, 2008) pp. 277–356.
 - ²² X. Y. Xu, Y. Qi, J. Liu, L. Fu, and Z. Y. Meng, Phys. Rev. B **96**, 041119 (2017).
 - ²³ L. Wang, ArXiv e-prints (2017), arXiv:1702.08586 [physics.comp-ph].
 - ²⁴ L. Huang, Y.-f. Yang, and L. Wang, Phys. Rev. E **95**, 031301 (2017).
 - ²⁵ R. T. Scalettar, D. J. Scalapino, R. L. Sugar, and D. Toussaint, Phys. Rev. B **36**, 8632 (1987).
 - ²⁶ S. Duane, A. D. Kennedy, B. J. Pendleton, and D. Roweth, Phys. Lett. **B195**, 216 (1987).
 - ²⁷ A. Kennedy and B. Pendleton, Nuclear Physics B **607**, 456510 (2001).
 - ²⁸ J. Kogut and L. Susskind, Phys. Rev. D **11**, 395 (1975).
 - ²⁹ S. R. White, R. L. Sugar, and R. T. Scalettar, Phys. Rev. B **38**, 11665 (1988).
 - ³⁰ M. Bercx, F. Goth, J. S. Hofmann, and F. F. Assaad, ArXiv e-prints (2017), arXiv:1704.00131 [cond-mat.str-el].
 - ³¹ A. J. Heeger, S. Kivelson, J. R. Schrieffer, and W. P. Su, Rev. Mod. Phys. **60**, 781 (1988).
 - ³² A. N. Rubtsov, V. V. Savkin, and A. I. Lichtenstein, Phys. Rev. B **72**, 035122 (2005).
 - ³³ F. F. Assaad and T. C. Lang, Phys. Rev. B **76**, 035116 (2007).
 - ³⁴ F. F. Assaad, “Dmft at 25: Infinite dimensions: Lecture notes of the autumn school on correlated electrons,” (Verlag des Forschungszentrum Jülich, Jülich, 2014) Chap. 7. Continuous-time QMC Solvers for Electronic Systems in Fermionic and Bosonic Baths, iISBN 978-3-89336-953-9.
 - ³⁵ M. Hohenadler and T. C. Lang, “Autocorrelations in quantum monte carlo simulations of electron-phonon models,” in *Computational Many-Particle Physics*, edited by H. Fehske, R. Schneider, and A. Weiße (Springer Berlin Heidelberg, Berlin, Heidelberg, 2008) pp. 357–366.
 - ³⁶ J. Hirsch, Phys. Rev. B **28**, 4059 (1983).
 - ³⁷ J. E. Hirsch, Phys. Rev. B **31**, 4403 (1985).
 - ³⁸ J. S. Liu, *Monte Carlo Strategies in Scientific Computing* (Springer New York, 2004).
 - ³⁹ E. Hairer, C. Lubich, and G. Wanner, *Geometric Numerical Integration: Structure-Preserving Algorithms for Ordinary Differential Equations: 31 (Springer Series in Computational Mathematics)* (Springer, 2006).
 - ⁴⁰ E. Hairer and G. Söderlind, SIAM Journal on Scientific Computing **26**, 18381851 (2005).
 - ⁴¹ Z. Bai, W. Chen, R. Scalettar, and I. Yamazaki, in *Multi-scale Phenomena in Complex Fluids: Modeling, Analysis and Numerical Simulation*, edited by T. Y. Hou (World Scientific, 2009).
 - ⁴² I. Yamazaki, Z. Bai, W. Chen, and R. Scalettar, Numerical Mathematics: Theory, Methods and Applications **2**, 469 (2009).
 - ⁴³ S. R. White and J. W. Wilkins, Phys. Rev. B **37**, 5024 (1988).
 - ⁴⁴ S. Chakravarty, B. I. Halperin, and D. R. Nelson, Phys. Rev. Lett. **60**, 1057 (1988).
 - ⁴⁵ M. Hasenbusch, Physics Letters B **519**, 177 (2001).
 - ⁴⁶ M. A. Clark and A. D. Kennedy, Phys. Rev. Lett. **98**, 051601 (2007).
 - ⁴⁷ M. Weber, F. F. Assaad, and M. Hohenadler, Phys. Rev. B **91**, 245147 (2015).